

# Synthesis and Properties of Thermoelectric Nanomaterial AgInSe<sub>2</sub> with a Chalcopyrite Structure

A. E. Vasiliev<sup>a</sup>, O. N. Ivanov<sup>a,b</sup>, M. V. Zhezhu<sup>a</sup>, and M. N. Yaprntsev<sup>a,\*</sup>

<sup>a</sup> Belgorod State University, Belgorod, Russia

<sup>b</sup> Belgorod State Technological University, Belgorod, Russia

\*e-mail: yaprintsev@bsu.edu.ru

Received November 25, 2020; revised November 25, 2020; accepted December 8, 2020

**Abstract**—AgInSe<sub>2</sub> nanopowders with a chalcopyrite structure and an average particle size of ~75 nm were synthesized from solutions by the polyol method of chemical synthesis. Spark plasma sintering was used to obtain bulk polycrystalline nanomaterials with an average grain size of ~110 nm. Electrons are the main current carriers in bulk materials. In the range 300–700 K, the features of the temperature dependences of the electrical resistivity, Seebeck coefficient, and total thermal conductivity of the nanomaterials are determined. It was found that the maximum thermoelectric figure of merit, equal to 0.1, is achieved at a temperature of 700 K.

DOI: 10.1134/S2635167621030198

## INTRODUCTION

Global warming, caused mainly by the burning of fossil fuels, is one of the most important and urgent problems of our time [1]. Most of the currently used energy conversion methods are not highly efficient, they all have large amounts of heat loss. Therefore, it is imperative to find reliable ways to recover waste heat without interruption. Thermoelectric generation is a simple and environmentally friendly solution for the direct conversion of thermal energy into electrical energy [2–5]. In addition to solving the environmental problem, the use of thermoelectric power generation allows the power supply of low-power devices and sensors in places that are difficult to access for laying a centralized network power supply [6, 7]. Also, thermoelectric devices can be widely used for local cooling (or heating) by creating electric solid-state heat pumps. Thermoelectric devices have no moving parts in their design, which makes them more reliable than other options, do not emit greenhouse gases (freon, CO<sub>2</sub>) and can be subject to miniaturization [8].

Thermoelectric efficiency of materials is determined by the thermoelectric figure of merit  $ZT$ , which can be expressed as  $ZT = S^2T/k\rho$ , where  $T$  is the absolute temperature,  $S$  is the Seebeck coefficient,  $\rho$  is the electrical resistivity, and  $k$  is the total thermal conductivity, including lattice and electronic contributions. To achieve high values of  $ZT$  thermoelectric materials must simultaneously have low thermal conductivity and electrical resistivity and a high Seebeck coefficient. These thermoelectric properties are closely related to each other, and usually the improvement of

some properties negatively affects others, which significantly limits their simultaneous optimization [9–14]. In addition to improving the properties of traditional thermoelectric materials (compounds based on Bi<sub>2</sub>Te<sub>3</sub>, SiGe and PbTe [15–17]), research is currently underway to develop new compounds with a complex structure (skutterudites, clathrates, semi-heislars, etc.), which can be promising for TE applications [15–26].

Complex chalcogenides with a chalcopyrite structure (sp.gr.  $\bar{I}42d$  (no. 122)) have low lattice thermal conductivity [21], which contributes to the achievement of high thermoelectric efficiency. To control the electrical properties of chalcogenides, doping in the cation sublattice is used [23–25]. To obtain materials based on complex chalcogenides, the method of solid-state synthesis from pure elements is often used [23–25], which, firstly, requires the use of expensive organic solvents and auxiliary substances, which are environmentally unsafe and require special disposal measures when introduced into production. [26–29], and, secondly, makes it difficult to obtain nanostructured materials (it is known that nanostructuring is one of the most effective ways to increase the thermoelectric figure of merit of materials [30]).

The aim of this study is to develop a simple, efficient, and scalable method for the preparation of nanoparticles of complex chalcogenides using the example of the AgInSe<sub>2</sub> designed to obtain bulk thermoelectric materials.

## EXPERIMENTAL

To obtain the initial  $\text{AgInSe}_2$  powder we used a polyol method of chemical synthesis from solutions. This method is based on the use of metal salts dissolved in polyhydric alcohols, which are polyols (ethylene glycol, glycerin, diethylene glycol, polyethylene glycol). Analytically pure chemicals ( $\text{AgNO}_3$ ,  $\text{In}(\text{NO}_3)_3 \cdot 5\text{H}_2\text{O}$ ,  $\text{SeO}_2$ , ethylene glycol (ethane-1,2-diol)) and glycerin (propanetriol-1,2,3). Initial substances taken in a stoichiometric ratio per 10 g of  $\text{AgInSe}_2$ , was dissolved in 300 mL of ethylene glycol or glycerin in a round-bottom flask with moderate heating ( $80^\circ\text{C}$ ) and constant stirring. After complete dissolution of the precursors, the reaction mixture was heated to  $180^\circ\text{C}$  (for ethylene glycol) or to  $250^\circ\text{C}$  (for glycerol). When the specified temperature of the reaction medium was reached, a reflux condenser was installed to condense the rising vapors. The reaction system was kept at a given temperature for 3 h. After cooling the reaction medium to room temperature, the resulting powder was separated by vacuum filtration, followed by washing the resulting powder with hot ethyl alcohol to remove reaction by-products. The powder was dried in an inert atmosphere at  $150^\circ\text{C}$  for 8 h. To obtain bulk materials from synthesized powders, the method of spark plasma sintering (SPS) was used using the SPS-25 system at a temperature of  $700^\circ\text{C}$ , a pressure of 40 MPa, and a sintering time of 30 min.

Electron microscopic studies of the initial powders were carried out with a JEM-2010 (JEOL) transmission electron microscope (TEM). The density of bulk samples was measured by the Archimedes method. For XRD analysis of initial powders and bulk samples, a Rigaku Ultima IV X-ray powder diffractometer was used ( $\text{CuK}\alpha$  radiation, Ni-filter). The phases were identified using the PDF powder X-ray standards database (JCPDS ICDD). The crystal lattice was indexed by the methods of graphical analysis, and the lattice parameters were calculated using the PDXL software (RIGAKU). A Nova NanoSEM 450 (FEI) scanning electron microscope (SEM) was used to study the features of the grain structure of bulk samples. The electrical resistivity and Seebeck coefficient of bulk samples were measured using the ZEM-3 system, and the total thermal conductivity was measured using the TC-1200 system.

## RESULTS AND DISCUSSION

At the first stage of the study, the effect of the type of solvent (and at the same time a reducing agent), ethylene glycol or glycerin, on the phase composition, crystal structure, and particle shape of the initial  $\text{AgInSe}_2$  powder designed to obtain bulk material was studied.

According to the XRD data (Fig. 1a) during the synthesis of  $\text{AgInSe}_2$  in an ethylene glycol medium,

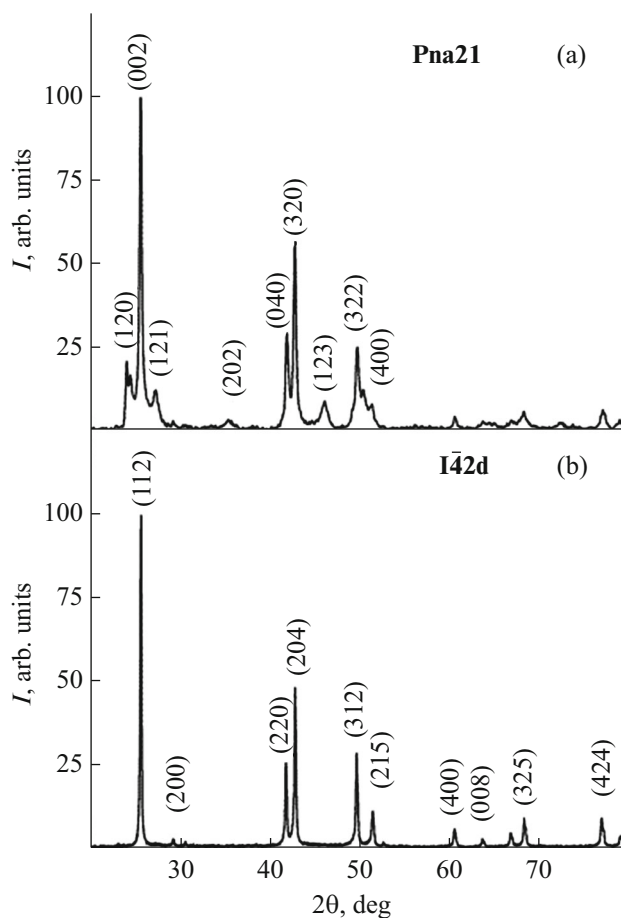
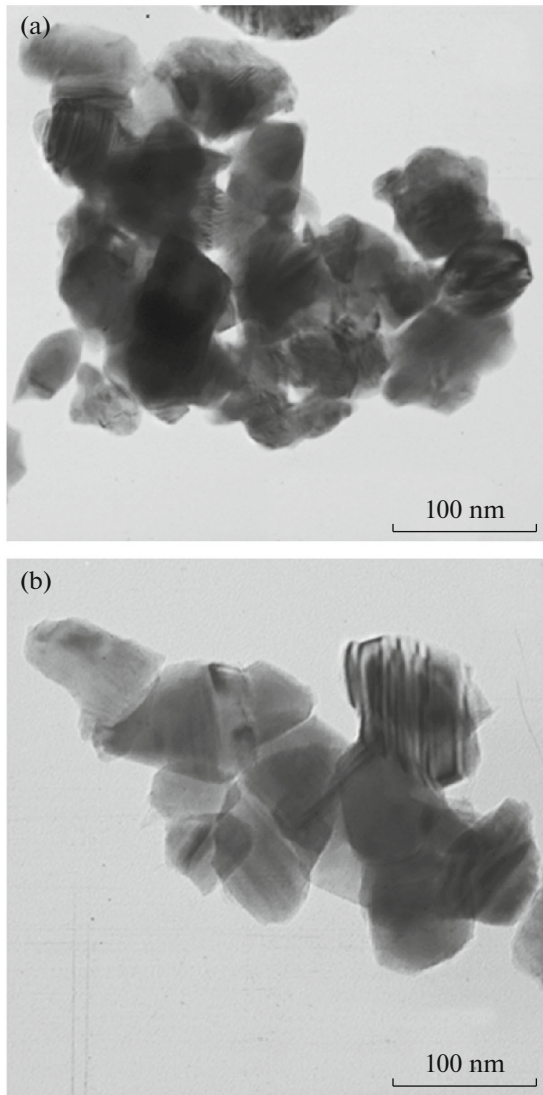


Fig. 1. Powder X-ray diffraction patterns of  $\text{AgInSe}_2$  obtained in an ethylene glycol medium at  $180^\circ\text{C}$  (a) and in a glycerol medium at  $250^\circ\text{C}$  (b).

the obtained powder materials have orthorhombic crystal lattice  $\text{AgInSe}_2$  (sp. gr.  $Pna21$  (no. 33), which is isostructural to the well-known  $\text{AgInS}_2$  phase (JCPDS-00-025-1328). Thus, when using ethylene glycol, a phase with the desired chalcopryrite structure is not formed. It was shown in [27] that the type of crystal structure of  $\text{AgInSe}_2$  formed during chemical synthesis depends on the synthesis temperature of the initial powder. To raise the synthesis temperature, instead of ethylene glycol, another solvent with a higher boiling point is needed. Therefore, in the subsequent synthesis, glycerol was used as a solvent, which made it possible to increase the synthesis temperature to  $250^\circ\text{C}$  without additional auxiliary chemicals and complex, expensive equipment (autoclaves, high-pressure reactors, etc.). It was found by XRD that synthesis under these conditions makes it possible to obtain single-phase  $\text{AgInSe}_2$  powders (pr. gr.  $I42d$  (no. 122)) with a chalcopryrite structure (JCPDS-03-065-6377) with unit cell parameters  $a = b = 6.095$  and  $c = 11.638 \text{ \AA}$  (Fig. 1b).



**Fig. 2.** TEM images of  $\text{AgInSe}_2$  obtained in an ethylene glycol medium at  $180^\circ\text{C}$  (a) and in a glycerol medium at  $250^\circ\text{C}$  (b).

The results of studying the powders synthesized in both ethylene glycol and glycerol media by transmission electron microscopy are shown in Fig. 2. It can be seen that in both cases the powder is represented by irregular nanoparticles. It is also seen that an increase in temperature from 180 to  $250^\circ\text{C}$  leads to an increase in the average particle size from 50 to 75 nm. Analysis of the synthesized powders by energy dispersive X-ray spectroscopy showed that in both cases the elemental composition corresponds to the specified one ( $\omega(\text{Ag}) = 24.97$ ,  $\omega(\text{In}) = 25.12$ ,  $\omega(\text{Se}) = 49.91$  at %).

To obtain bulk samples, the synthesized  $\text{AgInSe}_2$  powder with a chalcopyrite structure was compacted by SPS. The density of bulk samples is  $5.3 \text{ g/cm}^3$ , which is  $\sim 91\%$  of the theoretical density ( $5.82 \text{ g/cm}^3$  according to [31]).

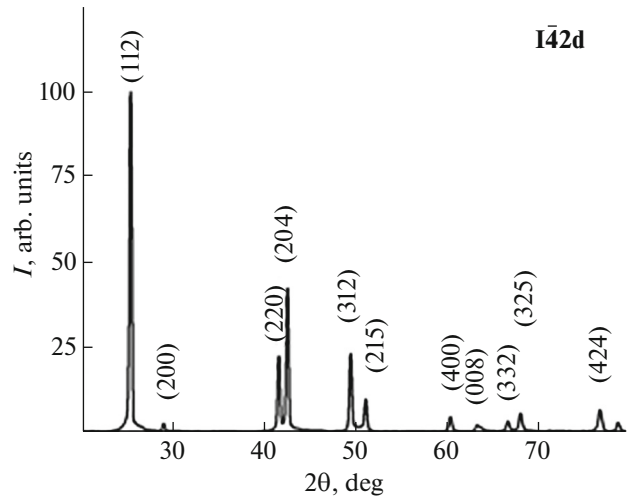


**Fig. 3.** Powder X-ray diffraction pattern of a bulk  $\text{AgInSe}_2$  sample with the structure of chalcopyrite obtained by SPS.

Figure 3 shows the diffractogram of the obtained volumetric sample. It can be seen that during sintering the crystal structure of chalcopyrite with the unit cell parameters corresponding to the initial powder is retained. It was also found that, during sintering, there is an insignificant change in the elemental composition in comparison with the initial powder (the content of Ag, In, and Se in the bulk material is 25.19, 24.86, and 49.95 at % respectively).

Figure 4 shows SEM images of the cleavage surface of a bulk sample. The sample is characterized by a disordered grain structure with irregular grains. To estimate average grain size  $D$  a histogram of grain size distribution was plotted (Fig. 4). For its construction, the sizes of 100 grains were used. It was found that the histogram can be satisfactorily described in terms of a lognormal unimodal distribution. The probability density of a lognormal distribution is expressed as

$$F(D) = \frac{1}{\sqrt{2\pi}\sigma D} \exp\left(-\frac{(\ln D - \ln D_a)^2}{2\sigma^2}\right), \quad (1)$$

where  $\sigma$  is the standard deviation of the grain size from the average size (the width of the grain size distribution).

The value of  $D$  was  $\sim 110$  nm and the standard deviation was  $\pm 41$  nm. Thus, the average grain size in the bulk material is about 50% larger than the average particle size in the original powder. Nevertheless, we can assume that the value of  $D$  corresponds to a nanomaterial (material with a nano-grained structure).

Figure 5 shows the temperature dependences of the electrical resistivity (a) and the Seebeck coefficient (b) of a bulk sample. It can be seen that with an increase in temperature in the range 300–700 K, a decrease in the specific electrical resistance by more than 120 times is observed, from 0.12 (300 K) to  $9.8 \times$

$10^{-4} \Omega \text{ m}$  (700 K). This behavior is typical for nondegenerate semiconductors and is caused by an increase in the concentration of current carriers with increasing temperature. In the same interval, the Seebeck coefficient monotonically increases with an increase in temperature from  $-57$  (300 K) to  $-225 \mu\text{V K}^{-1}$  (700 K). Since the Seebeck coefficient has a negative value over the entire temperature range, it can be argued that the material under study is a semiconductor of  $n$ -type. The appearance of electrons as the main current carriers in  $\text{AgInSe}_2$  associated with the formation of vacancies in Se at high temperatures, which, in turn, is due to the evaporation of selenium. For non-degenerate semiconductors with  $n$ -type conductivity of the Seebeck coefficient is determined by expression

$$S = \frac{2k_B^2 T m^*}{3e\hbar^2} \left( \frac{\pi}{3n} \right)^{2/3}, \quad (2)$$

where  $k_B$  is the Boltzmann constant,  $e$  is the electron charge,  $\hbar$  is Planck's constant,  $m^*$  is the effective mass of the density of state for the conduction band, and  $n$  is the concentration of electrons.

In accordance with expression (2), the Seebeck coefficient should increase with increasing temperature, which was observed in the experiment (Fig. 5b). Note that in this case, the Seebeck coefficient is a negative value, and its increase refers to the absolute value. Minor dependency deviation  $S(T)$  on from the linear one can be associated with the temperature dependence of the electron concentration.

The temperature dependence of the total thermal conductivity of the sample is shown in Fig. 6. In the entire investigated temperature range, the value of  $k$  decreases from  $0.55$  (300 K) to  $0.32 \text{ W m}^{-1} \text{ TO}^{-1}$  (700 K). Taking into account the fact that, simultaneously with a decrease in the value of the specific thermal conductivity, a significant decrease in the specific electrical resistance occurs, it can be assumed that it is the lattice thermal conductivity that makes the main contribution to the total thermal conductivity. It is known that above the Debye temperature, the lattice thermal conductivity changes as  $T^{-1}$ . It is seen that experimental dependence  $k(T)$  in Fig. 6 qualitatively corresponds to this dependence. According to the Dulong–Petit law, above the Debye temperature, the lattice heat capacity does not depend on temperature, and the phonon energy increases linearly with increasing temperature. Since the probability of phonon scattering is proportional to their number, the lattice thermal conductivity decreases with increasing temperature as  $T^{-1}$ .

Temperature dependence  $ZT$  for a bulk sample of  $\text{AgInSe}_2$  with a chalcopyrite structure is shown in Fig. 7. This dependence can be divided into two sections. In the first section (in the range of 300–500 K), the thermoelectric figure of merit is very low (due to the high electrical resistance) and practically does not

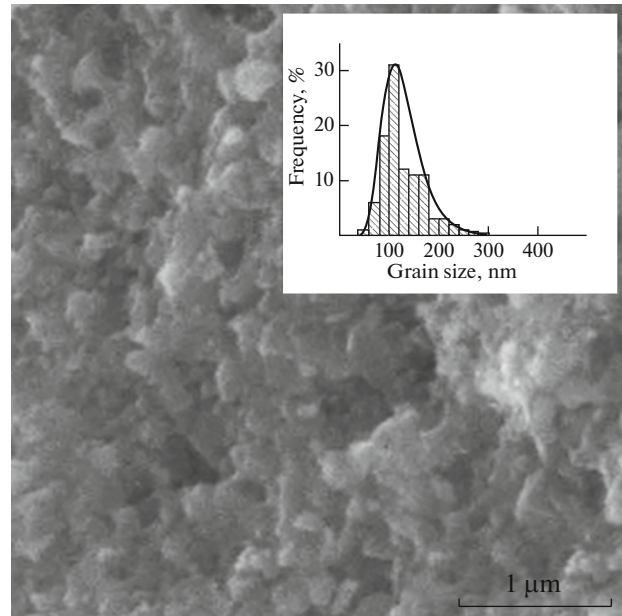


**Fig. 4.** SEM image of the cleavage surface of a bulk  $\text{AgInSe}_2$  sample with a chalcopyrite structure obtained by SPS. The inset shows a histogram of grain size distribution (the solid curve corresponds to the lognormal unimodal distribution).

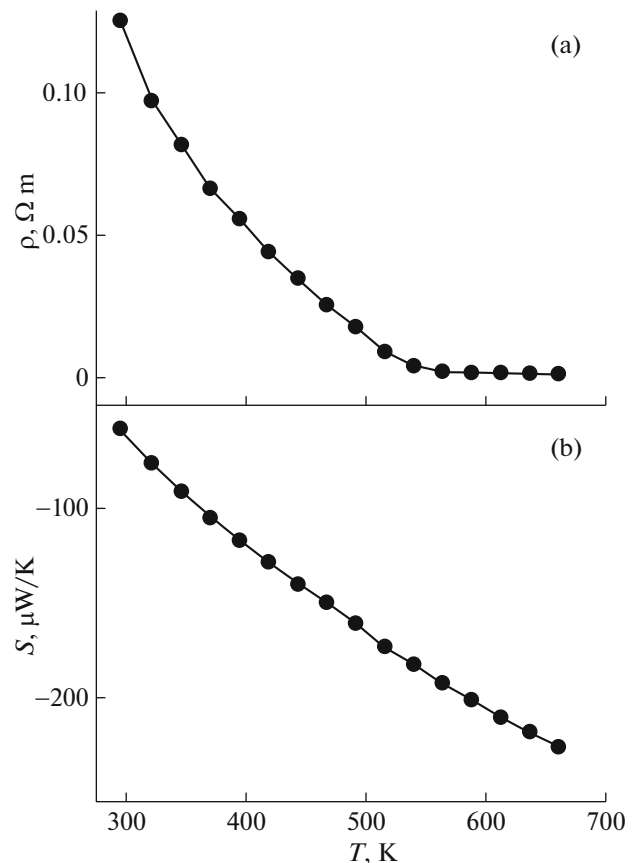


**Fig. 5.** Temperature dependences of electrical resistivity (a) and Seebeck coefficient (b).

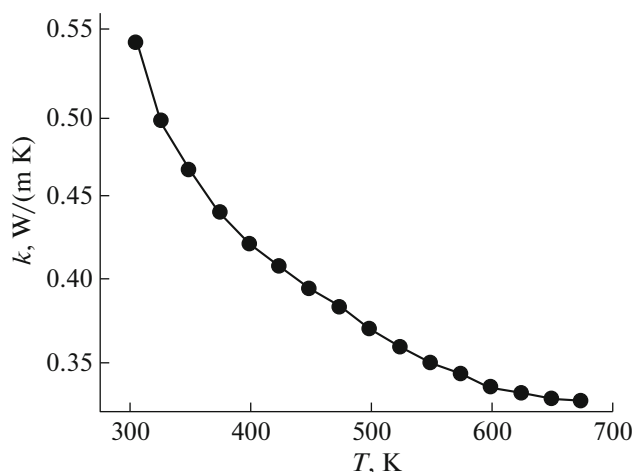


Fig. 6. Temperature dependence of the specific thermal conductivity of a bulk  $\text{AgInSe}_2$  sample with a chalcopyrite structure obtained by SPS.

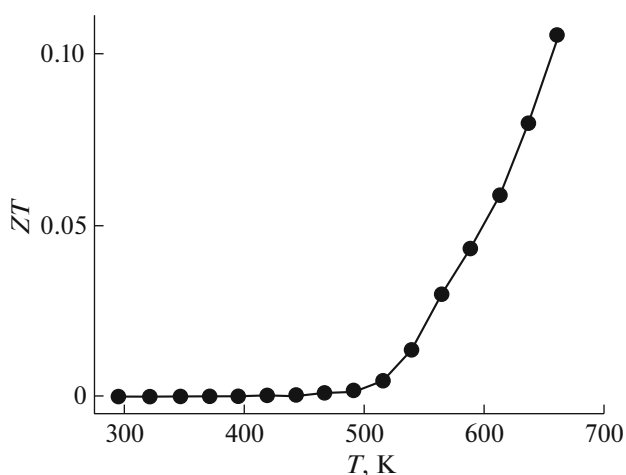


Fig. 7. Temperature dependence of the thermoelectric figure of merit of a bulk  $\text{AgInSe}_2$  sample with a chalcopyrite structure obtained by SPS.

depend on temperature. In the second section (above  $\sim 500$  K), a sharp increase in the thermoelectric figure of merit is observed (from 0.002 at 500 K to 0.1 at 700 K). This growth is mainly associated with a significant decrease in electrical resistance in a given temperature range. Despite the relatively low values of the thermoelectric figure of merit, the nanomaterial obtained in this study can be considered as a potentially effective medium-temperature thermoelectric. Since  $\text{AgInSe}_2$  with a chalcopyrite structure has a relatively low thermal conductivity, in order to improve the thermoelectric efficiency, it is advisable in the future to optimize the electrical transport properties, first of all, by alloying with various metals. Note that the proposed synthesis method allows doping of the resulting thermoelectric nanomaterial with various

elements at the stage of synthesis, both into the cationic sublattice (Bi, Zn, Cd, Pb, etc.) and into the selenium sublattice (Te, S). Also, this synthesis method can be adapted to obtain nanopowders of complex chalcogenides with a chalcopyrite structure of various compositions ( $\text{CuInTe}_2$ ,  $\text{CuSbSe}_4$ , etc.).

## CONCLUSIONS

A simple, efficient, and scalable method for the preparation of  $\text{AgInSe}_2$  nanoparticles is proposed with a chalcopyrite structure and an average nanoparticle size of  $\sim 75$  nm. A bulk polycrystalline material with an average grain size of  $\sim 110$  nm was obtained from the synthesized powder by SPS. The maximum value of the thermoelectric figure of merit of the bulk material ( $ZT \approx 0.1$ ) is achieved at a temperature of  $\sim 700$  K.

## FUNDING

This study was supported by the Ministry of Education and Science of the Russian Federation (project no. 0625-2020-0015).

## REFERENCES

1. R. Li, X. Li, L. Xi, et al., *ACS Appl. Mater. Interfaces* **11**, 24859 (2019). <https://doi.org/10.1021/acsami.9b01196>
2. L. E. Bell, *Science* (Washington, DC, U. S.) **321**, 1457 (2008). <https://doi.org/10.1126/science.1158899>
3. S. I. Kim, K. H. Lee, H. A. Mun, et al., *Science* (Washington, DC, U. S.) **348**, 109 (2015). <https://doi.org/10.1126/science.aaa4166>
4. L. D. Zhao, G. Tan, S. J. Hao, et al., *Science* (Washington, DC, U. S.) **351**, 141 (2016). <https://doi.org/10.1126/science.aad3749>
5. X. Shi and L. Chen, *Nat. Mater.* **15**, 691 (2016). <https://doi.org/10.1038/nmat4643>
6. V. Kh. Berdin, *Renewable Energy Sources in Isolated Settlements in the Russian Arctic* (Vsemirnyi Fond Dikoi Prirody (WWF), Moscow, 2017) [in Russian].
7. V. M. Rudoi, N. I. Ostanin, and Yu. P. Zaikov, *Design of Cathodic Protection of Underground Pipelines* (GOU VPO UGTU-UPI, Yekaterinburg, 2005) [in Russian].
8. N. P. Semena, *Thermophys. Aeromech.* **20**, 211 (2013).
9. H. J. Goldsmid, *Materials* **7**, 2577 (2014). <https://doi.org/10.3390/ma7042577>
10. W. Liu, X. Yan, G. Chen, et al., *Nano Energy* **1**, 42 (2012). <https://doi.org/10.1016/j.nanoen.2011.10.001>
11. Z. Xingyi, Y. Yue, L. Feng, et al., *Constr. Build. Mater.* **228**, 116818 (2019). <https://doi.org/10.1016/j.conbuildmat.2019.116818>
12. O. Ivanov, M. Yaprincev, R. Lyubushkin, et al., *Scr. Mater.* **146**, 91 (2018). <https://doi.org/10.1016/j.scriptamat.2017.11.031>

13. M. Yaprıntsev, R. Lyubushkin, O. Soklakova, and O. Ivanov, *J. Electron. Mater.* **47**, 1362 (2018).  
<https://doi.org/10.1007/s11664-017-5940-8>
14. O. Ivanov and M. Yaprıntsev, *Mater. Res. Express* **5**, 015905 (2018).  
<https://doi.org/10.1088/2053-1591/aaa265>
15. H. J. Goldsmid, *Thermoelectric Refrigeration, Electrical Engineering* (Springer, Boston, 2013).
16. W. X. Ni, W. M. Chen, I. A. Buyanova, et al., *J. Cryst. Growth* **157**, 242 (1995).
17. J. P. Heremans, V. Jovovic, E. S. Toberer, et al., *Science* (Washington, DC, U. S.) **321**, 554 (2008).  
<https://doi.org/10.1126/science.1159725>
18. X. Shi, J. Yang, J. Salvador, et al., *J. Am. Chem. Soc.* **133**, 7837 (2011).  
<https://doi.org/10.1021/ja111199y>
19. G. S. Nolas, *The Physics and Chemistry of Inorganic Clathrates* (Springer, Boston, 2014).
20. J. Yang, H. M. Li, T. Wu, et al., *Adv. Funct. Mater.* **18**, 2880 (2008).  
<https://doi.org/10.1002/adfm.200701369>
21. E. J. Skoug, J. D. Cain, and D. T. Morelli, *Appl. Phys. Lett.* **98**, 261911 (2011).  
<https://doi.org/10.1063/1.3605246>
22. N. Cheng, R. Liu, S. Bai, et al., *J. Appl. Phys.* **115**, 163705 (2014).  
<https://doi.org/10.1063/1.4872250>
23. W. G. Zeier, H. Zhu, Z. M. Gibbs, et al., *J. Mater. Chem. C* **2**, 10189 (2014).  
<https://doi.org/10.1039/C4TC02218A>
24. Y. Qin, P. Qiu, R. Liu, et al., *J. Mater. Chem. A* **4**, 1277 (2016).  
<https://doi.org/10.1039/C5TA09584K>
25. J. Zhang, R. Liu, N. Cheng, et al., *Adv. Mater.* **26**, 3848 (2014).  
<https://doi.org/10.1002/adma.201400058>
26. A. Yusufu, K. Kurosaki, A. Kosuga, et al., *Appl. Phys. Lett.* **99**, 061902 (2011).  
<https://doi.org/10.1063/1.3617458>
27. M. T. Ng, C. B. Boothroyd, and J. J. Vittal, *J. Am. Chem. Soc.* **128**, 7118 (2006).  
<https://doi.org/10.1021/ja060543u>
28. M.-A. Langevin, A. M. Ritcey, and C. N. Allen, *ACS Nano* **8**, 3476 (2014).  
<https://doi.org/10.1021/nn406439w>
29. O. Yarema, M. Yarema, and D. Bozyigit, *ACS Nano* **9**, 11134 (2015).  
<https://doi.org/10.1021/acsnano.5b04636>
30. A. J. Minnich, M. S. Dresselhaus, Z. F. Ren, et al., *Energy Environ. Sci.* **2**, 466 (2009).  
<https://doi.org/10.1039/b822664b>
31. O. Madelung, *Semiconductors: Data Handbook* (Springer, Berlin, 2004).  
<https://doi.org/10.1007/978-3-642-18865-7>